2023

High Figure of Merit Spin Polarized Electron Sources Grown Via MOCVD

Benjamin Belfore
Old Dominion University

Adam Masters
Old Dominion University, amast001@odu.edu

Deewakar Poudel
Old Dominion University, dpoud001@odu.edu

Greg Blume
Old Dominion University, gblum002@odu.edu

Stephen Polly
Rochester Institute of Technology

See next page for additional authors

Original Publication Citation

Belfore, B., Masters, A., Poudel, D., Blume, G., Polly, S., Wang, E., Hubbard, S. M., Stutzman, M., Grames, J. M., Poelker, M., Grau, M., & Marsillac, S. (2023). High figure of merit spin polarized electron sources grown via MOCVD. *Applied Physics Letters*, *123*(22), 1-6, Article 222102. https://doi.org/10.1063/5.0170106

Applied Physics Letters ARTICLE pubs.aip.org/aip/apl

High figure of merit spin polarized electron sources grown via MOCVD

Cite as: Appl. Phys. Lett. **123**, 222102 (2023); doi: 10.1063/5.0170106
Submitted: 31 July 2023 · Accepted: 8 November 2023 ·
Published Online: 27 November 2023

Benjamin Belfore,[1] Adam Masters,[1] Deewakar Poudel,[1] Greg Blume,[1] Stephen Polly,[2] Erdong Wang,[3] Seth M Hubbard,[2] Marcy Stutzman,[4] Joseph Michael Grames,[4] Matt Poelker,[4] Matt Grau,[1] and Sylvain Marsillac[1,a)]

AFFILIATIONS

[1]Old Dominion University, 5115 Hampton Blvd, Norfolk, Virginia 23529, USA
[2]Rochester Institute of Technology, 1 Lomb Memorial Drive, Rochester, New York 14623, USA
[3]Brookhaven National Laboratory, 2 Center Street, Upton, New York 11973, USA
[4]Thomas Jefferson National Accelerator facility, 12000 Jefferson Avenue, Newport News, Virginia 23606, USA

[a)]**Author to whom correspondence should be addressed:** smarsill@odu.edu

ABSTRACT

Spin polarized photocathodes are key to the future operation of electron accelerators such as the ones at Thomas Jefferson National Accelerator Facility and Brookhaven National Laboratory. Currently, these photocathodes come in short supply due to limited production by molecular beam epitaxy. By developing a process to implement similar structures using metal organic chemical vapor deposition, the availability of these devices can be increased. In this paper, we detail the implementation of recent photocathode advancements via metal organic chemical vapor deposition process and show an improvement in both polarization and quantum efficiency of our devices compared to those fabricated via molecular beam epitaxy, with devices reaching 82% polarization and 2.9% quantum efficiency.

Spin polarized electron sources have been integral to electron accelerators performing spin-physics studies. Since the first demonstration of spin polarized photoemission in 1976, significant efforts have been put into developing these photocathodes for accelerator applications.[1] For that reason, their development has gone hand in hand with accelerator development. Initial spin polarized photocathodes were created using commercially available p-type GaAs wafers, which can provide very high quantum efficiency (QE: ratio of electrons emitted to incident photons) in the range of 10% but spin polarization (degree to which the spin is aligned in a given direction) of only ∼35%. With such low polarization, considerably more beam time would be required to achieve the desired level of statistical uncertainty, and so a solution needed to be developed. Spin polarized electron sources have been integral to many high impact experiments performed at electron accelerators, including measurements of the strangeness distribution in the nucleon,[2,3] precision tests of the standard model,[4] a measurement of the neutron radius of 208Pb,[5] and the accurate determination of the ratio G_E/G_M for the proton[6] using the polarization transfer technique, and is an essential component to the future electron–ion collider[7] to explain how the mass of a proton originates. Due to its band structure, GaAs is inherently limited to 50% polarization[8] except if modified by compressive strain, allowing the heavy hole and light hole bands to split into two discrete bands, which offers a theoretical polarization up to 100%. This band splitting scheme was first proven using an InGaAs layer on a GaAs wafer, with polarization reaching 70%.[9] One of the main challenges of this process was the fact that the strain will begin to relax for layers beyond a critical thickness, resulting in misfit defects and poor optical and electrical film quality. Another issue is the lower quantum efficiency achieved by these devices[1] due in part to these defects, the lattice mismatch, and gradient in the orbital splitting energy.[10] To address this, superlattices were then grown, whereby a thin layer of the strained emitting material is sandwiched between a buffer material. Initial InGaAs/GaAs superlattice structures resulted in polarizations of 82% with quantum efficiencies near 0.015%.[11] While the quantum efficiency was still low, both the spin polarization and quantum efficiency showed notable increase over a strained epi-layer InGaAs on GaAs. Much similar to the strained epilayer system, when the materials were changed from the compressive InGaAs/GaAs system to tensile GaAsP/GaAs, both the spin polarization and quantum efficiency were improved. This improvement continued until photocathodes were developed with polarizations of 92% and quantum efficiencies

of 1.6%.[8] While this high degree of polarization is excellent, it would be better if quantum efficiency was higher, thus enabling experiments at much higher current.[6] Quantum efficiency is limited by multiple factors. First, while the superlattice does facilitate uniform strain through the emitting material, this barrier material in the superlattice does not emit spin polarized electrons. This means approximately half of the superlattice thickness emits no electrons. Furthermore, carefully controlling the barrier thickness is integral to prevent depolarization. Transport from within the photocathode to the surface itself can cause depolarization, so a balance must be made between the thickness of both the buffer layer and the number of periods in the superlattice.[8] To increase the thickness of the strained superlattice without changing its spatial dimensions, a distributed Bragg reflector (DBR) can be implemented. A DBR is a special type of a dielectric mirror where materials of alternating refractive indices are used to create a high degree of reflectivity over a range of optical wavelengths.[12] This results in a significant portion of the light that is not absorbed by the superlattice to be reflected back into the optical cavity formed between the DBR and the top surface, allowing for potentially several passes of laser light without actually increasing the active layer thickness. With the implementation of a DBR, our team has fabricated photocathodes with spin polarization of 84% and a QE of 6.4%.[8] The fabrication process used at the time was molecular beam epitaxy (MBE), which allows for the precise control of the strained superlattice photocathode, where layers are only 3–4 nm thick.

There are two common methods of photocathode fabrication: metal organic chemical vapor deposition (MOCVD) and MBE. As mentioned previously, for the photocathodes with spin polarizations of 84% and a QE of 6.4%, our team used MBE, which allows for precise control of the strain and thickness of the layers. However, some other studies have shown that the quality of the MOCVD grown photocathodes might be better due to the fact that the carrier build-up near the photocathode surface in the MOCVD device is more efficient compared to the MBE device.[13] It is also known that MBE is an expensive and slow fabrication tool, unlike MOCVD systems, which have higher growth rates and enhanced safety when growing phosphorus containing materials. The goal of this paper is, therefore, to demonstrate the use of MOCVD as a process for the fabrication of spin polarized electron devices with strained superlattice and DBR and compare them with similar devices fabricated via MBE.

The structure of the devices we fabricated is described in detail below and depicted in Fig. 1. It starts with a GaAs wafer p-doped with Zn at a concentration of nominally $1.1 \times 10^{19}\,\mathrm{cm}^{-3}$ and resistivity of $7 \times 10^{-3}\,\Omega\,\mathrm{cm}$. Substrate orientations of (100) on-axis, (100) 2° ⟨110⟩, and (100) 2° ⟨111⟩ A were investigated. First, a metamorphic graded buffer layer is deposited, with an initial composition of GaAs and an end composition of $GaAs_{0.65}P_{0.35}$. This grade used a step function to increase the phosphorus content by 2.5% per a 500 nm thick layer, including an overshoot layer (OSL) of $GaAs_{0.625}P_{0.375}$ and ending with a 2500 nm thick fallback layer of $GaAs_{0.65}P_{0.35}$, all nominally p-doped to $5 \times 10^{18}\,\mathrm{cm}^{-3}$.

The next layer is the DBR, which is a type of the superlattice structure, where materials of alternating refractive indices are deposited to create a highly reflective mirror.[12,14] The wavelength of peak reflectivity and the width of the resonance can be controlled through the thickness of each layer and the number of periods. In order to maintain lattice matching to $GaAs_{0.65}P_{0.35}$, we considered two ternary

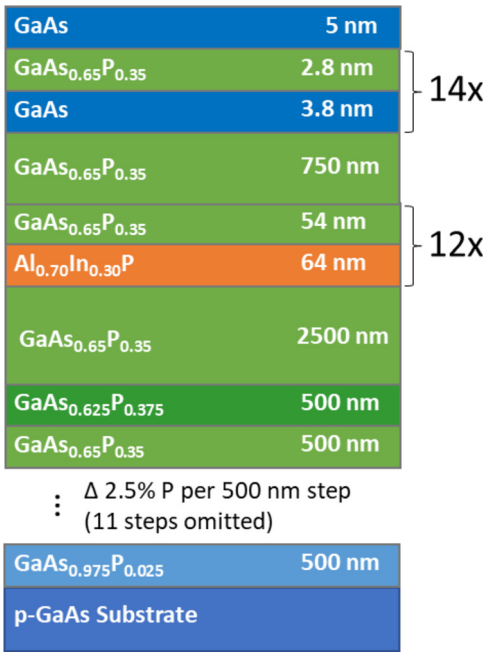

FIG. 1. Structure of the strained superlattice photocathode with DBR (not to scale).

semiconductor compounds to contrast with $GaAs_{0.65}P_{0.35}$ in the DBR: $AlAs_{0.61}P_{0.39}$ and $In_{0.30}Al_{0.70}P$. The $AlAs_{0.61}P_{0.39}$ compound has been used in the past to construct a similar DBR.[8] However, in a MOCVD system, $AlAs_{0.61}P_{0.39}$ has further complications due to its chemical instability. Indeed, if $AlAs_{0.61}P_{0.39}$ comes in contact with water vapor, it spontaneously and rapidly decomposes into Al_2O_3 and PH_3.[15] Another issue with $AlAs_{0.61}P_{0.39}$ is the non-linearity of PH_3 and AsH_3 incorporation. For these reasons, we opted for $In_{0.30}Al_{0.70}P$ instead, which due to the very similar dielectric functionality at the target central DBR wavelength should perform the same as $AlAs_{0.61}P_{0.39}$. The DBR was, therefore, composed of 12 pairs of $GaAs_{0.65}P_{0.35}$ and $In_{0.30}Al_{0.70}P$ with nominal thicknesses of 54 and 64 nm, respectively, and p-type Zn doping of $5 \times 10^{18}\,\mathrm{cm}^{-3}$.

After the DBR, another unstrained $GaAs_{0.65}P_{0.35}$ buffer layer with p-type Zn doping of $5 \times 10^{18}\,\mathrm{cm}^{-3}$ was deposited with a thickness of 0.75 μm. The next layer is the active layer of the photocathode. The superlattice is composed of alternative layers of strained GaAs and unstrained $GaAs_{0.65}P_{0.35}$, with nominal thicknesses of 3.8 and 2.8 nm, respectively, and p-type Zn doping of $5 \times 10^{17}\,\mathrm{cm}^{-3}$. Finally, 5 nm of strained GaAs was deposited with p-type C doping of $5 \times 10^{19}\,\mathrm{cm}^{-3}$.

Another photocathode was fabricated without a DBR, whereby the intermediate buffer layer is 2.75 μm. This will allow for the specific effect of the DBR to be measured.

These growths were performed in an Axitron close-coupled shower head MOCVD reactor. The key precursors used for these growths were trimethylgallium (TMGa), trimethylindium (TMIn), and trimethylaluminum (TMAl) for the group III elements, arsine and phosphine for the group V elements, and diethylzinc and carbon tetrachloride as the p-type doping agent. TMGa, AsH_3, and PH_3 were used as the main components in both the metamorphic graded buffer and

the strained superlattice. TMIn and TMAl were used to create the compounds of the distributed Bragg reflector.

During the fabrication runs, multiple parameters and substrates were used to obtain a fully relaxed metamorphic grading, which is necessary to grow defect-free DBR and superlattice structures. Three different (100) GaAs substrates were used: on-axis and 2° offcuts in the (110) and (111)A directions. While higher angle offcuts can improve relaxation, higher offcuts are detrimental to the final strained superlattice.[16] *In situ* measurements (growth rate, temperature, and reflectivity) were performed using a LayTec EpiCurveTT system. High-resolution x-ray diffraction (XRD) was used to corroborate film thickness as well as determine lattice constant and material composition. Hall effect measurements using the Van der Pauw method were used to determine the doping concentration. Nomarski microscopy was used to analyze the surface topography of grown samples. Transmission electron microscopy measurements were performed to evaluate crystalline quality, film thickness, and composition.

Every layer in the entire device structure is important, but the metamorphic graded layer has a special role as it is the one that will allow for low defect density strained GaAs layers to be grown on top of unstrained $GaAs_{0.65}P_{0.35}$ layers. This requires precise control of the metamorphic graded layer composition and lattice relaxation, which were controlled using growth temperature and precursor gas partial pressures. Temperature has two distinct impacts on the growth properties. As temperature rises, the deposited film will have more thermal energy potentially facilitating relaxation. Also, depending on the temperature, AsH_3 and PH_3 will incorporate differently because the rate of pyrolyzation of the hydrides is highly temperature dependent. At lower temperatures, AsH_3 will thermally decompose much faster than PH_3, leaving growth films that are significantly arsenic rich. The incorporation of phosphorous in the final film was, therefore, measured as a function of inlet gas compositions for various substrate temperatures, using reciprocal space mapping plots generated from XRD data. These data were fit using a Langmuir adsorption model and used for further precise control of GaAsP composition.

Once the composition was controlled (for a particular substrate temperature), the other key parameter to study was the effect of the wafer substrate orientation on the metamorphic graded layer relaxation. To ensure proper lattice relaxation within this metamorphic grading, the buffer layers were analyzed via high resolution x-ray diffraction techniques. In particular, asymmetrical (224) glancing exit (GE) reciprocal space maps were used. The first type of wafers we used was (100) GaAs with specific offcuts. The initial offcut was ⟨110⟩, but full relaxation was not obtained. To improve relaxation further, the offcut of the wafer was changed from the ⟨110⟩ direction to the ⟨111⟩ direction. This was done because the ⟨111⟩ step aligns better with the glide angle of defects within GaAs.[17] A reciprocal space mapping plot for the (100) GaAs substrate with 2° ⟨111⟩ A offcut is shown in Fig. 2 (left). As one can see, the metamorphic graded layer is nearly fully relaxed (99.8% relaxed, with a phosphorus composition of 36.2%). In contrast, the (100) on-axis wafers (Fig. 2, right) showed 90.1% relaxation at a composition of 41.2% phosphorus. Nomarski microscopy images indicated that both types of wafer orientation lead to smooth and uniform surfaces. Thus, there were two reasonable choices in terms of substrate orientation.

After the completion of the metamorphic graded layer, where the appropriate composition of $GaAs_{0.65}P_{0.35}$ and proper strain relaxation were obtained, the focus shifted to the growth of the DBR, where we chose $In_{0.30}Al_{0.70}P$ as the optical partner for this reflector, as discussed previously. To allow for a better comparison with the devices fabricated with molecular beam epitaxy, the choice was also made to keep the thicknesses of each layer and the total number of layers identical to our previous work.[8] It is, therefore, understood that the DBR is not yet optimized for the devices fabricated in this work. As can be seen from Fig. 3 (left), the transmission electron microscopy image indicates that the overall structure seems strain free, which is a requirement to grow a functional superlattice with unstrained $GaAs_{0.65}P_{0.35}$ and strained GaAs. Approximate thicknesses extracted from these images indicate that each of the $GaAs_{0.65}P_{0.35}$ and $In_{0.30}Al_{0.70}P$ layers is of the order of 51 and 62 nm, respectively, compared to targeted thicknesses of 54 and 64 nm. Energy dispersive x-ray spectroscopy measurements were done on the full structure and contrast images were generated (Fig. 3, center and right). Composition for each layer was found in good agreement with the targeted value and was confirmed with XRD, while mapping

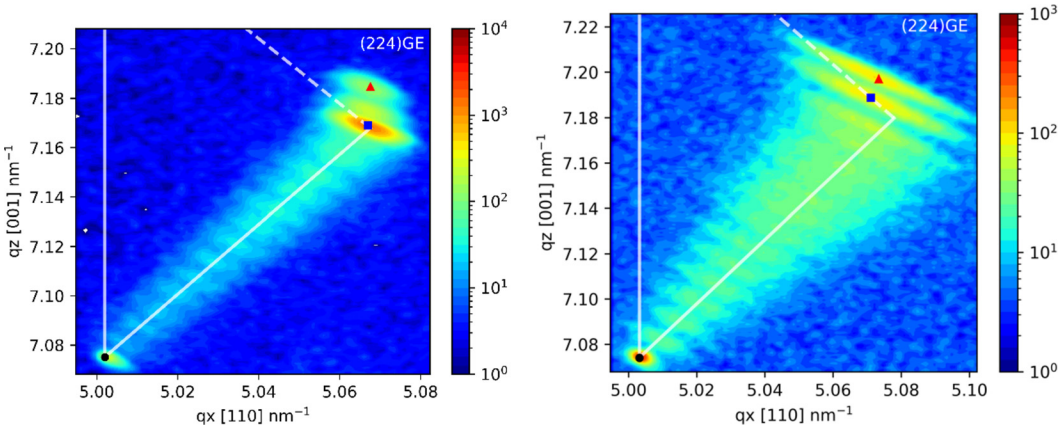

FIG. 2. (224) Glancing exit reciprocal space map for metamorphic graded layers grown on (100) GaAs wafer 2° ⟨111⟩ A offcut (left) and (100) on axis (right). Markers are shown for the substrate (black circle), overshoot layer (red triangle), and fallback layer (blue square), with the material relaxation line shown as dashed lines with endpoints of fully strained (vertical of the substrate) and fully relaxed (near the fallback layer) GaAsP on GaAs.

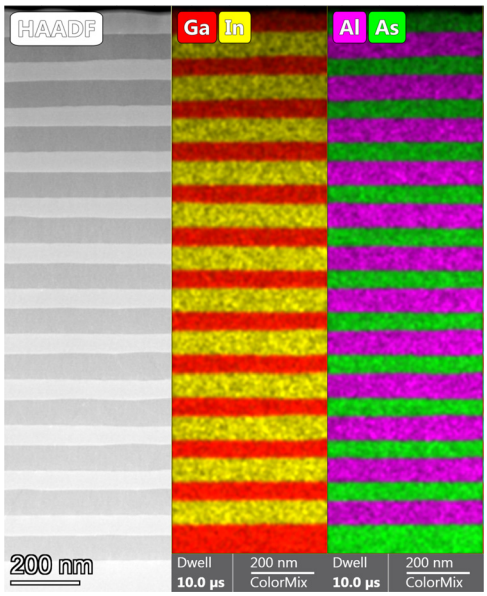

FIG. 3. Transmission electron microscopy image (left) and energy dispersive x-ray spectroscopy images (center and right) of the distributed Bragg reflector, composed of a sequence of $GaAs_{0.65}P_{0.35}$ and $In_{0.30}Al_{0.70}P$ layers.

indicates no inter-diffusion among the elements. Finally, reciprocal space mapping measurements were made and confirmed the proper relaxation of all the layers.

Once the distributed Bragg reflector was grown with the appropriate composition, thickness, and relaxation, the main task remaining was the growth of the spin emitter superlattice. This superlattice, which is the core spin polarized electrons generator for the entire structure, is nominally composed of 12 pairs of strained GaAs and unstrained $GaAs_{0.65}P_{0.35}$, of thicknesses 3.8 and 2.8 nm, respectively. Two types of wafers were used for this last study, based on the metamorphic graded layer results: (100) GaAs wafers with 2° ⟨111⟩ A offcut and on-axis (100) GaAs wafers.

The effect of the wafer orientation was studied by transmission electron microscopy (Fig. 4). As one can see, there is a significant impact on the fidelity of the superlattice. Specifically, for the (100) GaAs wafers with 2° ⟨111⟩ A offcut, the thicknesses of each layer are of the correct order of magnitude, but there are lateral non-uniformities occurring (the left image). This is likely caused by interfacial strain buildup at step edges, leading to step bunching and increased morphology.[18] On the other hand, for the on-axis (100) GaAs wafer, the layers are uniform in thickness throughout the width, with thicknesses for strained GaAs and unstrained $GaAs_{0.65}P_{0.35}$ of the order 4.2 and 3.1 nm, respectively, near the target values within the degree of measurement uncertainty (the right image).

Based on the results described above, we chose to deposit the full device on (100) on axis GaAs wafer. Photocathode samples were evaluated using a low voltage retarding-field Mott polarimeter.[19] Samples were attached to sample holders and installed within the vacuum chamber, which was baked under vacuum at 250 °C for 36 h and allowed to cool to room temperature. A negative electron affinity condition was obtained using the standard yo–yo activation procedure with cesium and NF_3.[20] This procedure was repeated twice (labeled first and second activation). A broadly tunable super-continuum laser (NKT Photonics, SuperK) provided the milli-Watts of output power over the wavelength range from 400 to 800 nm. Optical waveplates (quarter and halfwave) were used to generate the left and right circularly polarized light required to obtain spin polarized electrons.

Measured values of QE and electron-spin polarization (ESP) as a function of wavelength, for photocathodes with and without DBR, are shown in Fig. 5. For the non-DBR photocathode, the peak polarization is around 79% and the QE around 0.4% at a wavelength of 780 nm. This is lower than previous results for a similar structure and indicates that further refinement of the layer thicknesses and composition/strain in the superlattice is possible. However, as seen Fig. 5, the quantum efficiency for the sample with the distributed Bragg reflector is significantly higher than that for the one without, with values reaching as high as 2.9%. This is the second highest reported quantum efficiency for a strained superlattice photocathode.

These results are compared to results from other photocathodes listed in Table I, showing QE, polarization (P), and photocathode figure of merit, calculated by multiplying the square of the polarization by the quantum efficiency (P^2QE). The figure of merit of our photocathode is the second highest value reported overall and the highest value reported for a photocathode grown by MOCVD.

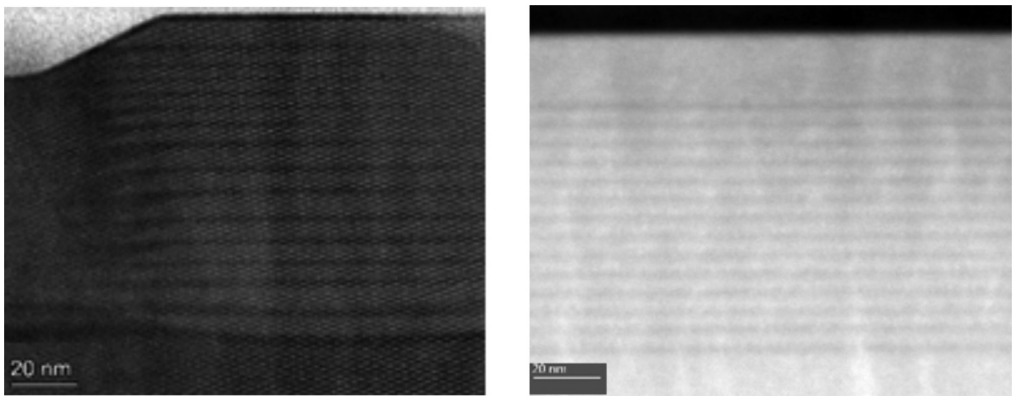

FIG. 4. Transmission electron microscopy images for the spin emitter superlattice layers grown on (100) GaAs wafer 2° ⟨111⟩ A offcut (left) and on axis (right).

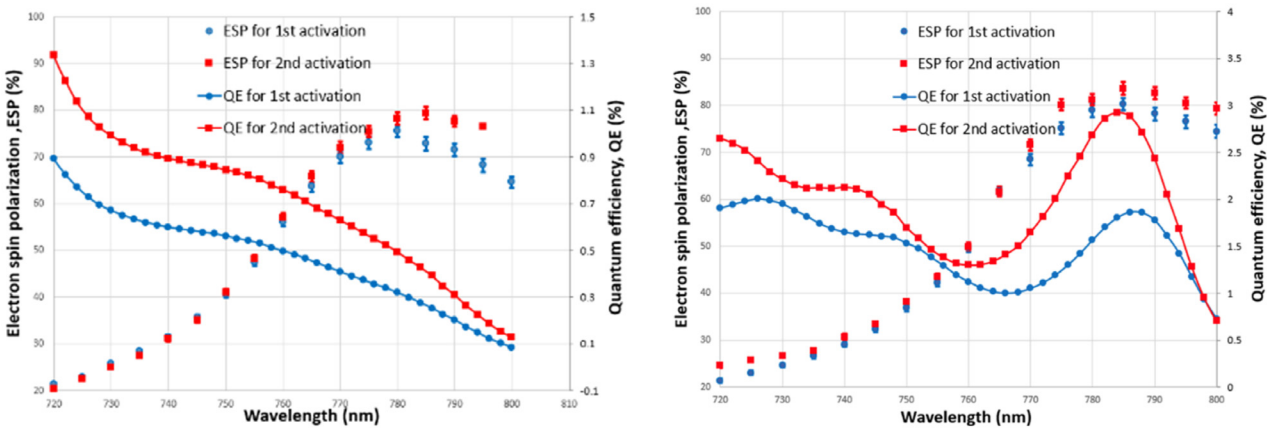

FIG. 5. The QE and electron-spin polarization (ESP) for the strained GaAs/GaAsP superlattice photocathodes without (left) and with (right) DBR as a function of the wavelength.

TABLE I. Figure of merit for polarized electron sources.

Material	Type	Growth process	Reference	Year	Wavelength (nm)	Maximum P (%)	QE (%) at Max P	Figure of merit (P^2QE) (%)
GaAs-$GaAs_{0.64}P_{0.36}$	Std	MOCVD	Watanabe *et al.*[21]	2001	780	92	0.2	0.17
GaAs-$GaAs_{0.64}P_{0.36}$	Std	MBE	Maruyama *et al.*[22]	2004	775	86	1.2	0.89
GaAs-$GaAs_{0.62}P_{0.38}$	Std	MBE	Jin *et al.*[23]	2014	780	92	1.6	1.35
GaAs-$GaAs_{0.65}P_{0.35}$	DBR	MBE	Liu *et al.*[8]	2016	776	84	6.4	4.52
GaAs-$GaAs_{0.65}P_{0.35}$	Std	MOCVD	This work	2022	785	79	0.4	0.25
GaAs-$GaAs_{0.65}P_{0.35}$	DBR	MOCVD	This work	2022	785	82	2.9	1.95

As Table I shows, our devices' polarization, with or without DBR, is lower than that for the devices grown by MBE reported here.[8,22,23] However, previous experiments have shown that devices grown by MOCVD can reach polarization as high as 92%.[21] When adding the DBR, the devices described here have the second highest figure of merit reported but are still behind devices our team grew by MBE by a factor of around 2.3.[8] Further optimization of the growth process with the help of device modeling should lead to higher QE and polarization values approaching the best values from superlattice photocathodes grown by MBE.

This material is based upon the work supported by the U.S. Department of Energy, Office of Science, Office of Nuclear Physics under Contract Nos. DE-AC05-06OR23177 and DE-SC0023369.

AUTHOR DECLARATIONS

Conflict of Interest

The authors have no conflicts to disclose.

Author Contributions

Benjamin Belfore: Conceptualization (equal); Formal analysis (equal); Investigation (equal); Writing – original draft (equal). **Matt Poelker:** Formal analysis (equal); Funding acquisition (equal); Investigation (equal); Writing – review & editing (equal). **Matt Grau:** Formal analysis (equal); Investigation (equal); Supervision (equal); Writing – review & editing (equal). **Sylvain Marsillac:** Conceptualization (equal); Funding acquisition (equal); Project administration (equal); Supervision (equal). **adam masters:** Investigation (equal); Writing – original draft (equal). **Deewakar Poudel:** Investigation (equal); Writing – review & editing (equal). **greg blume:** Formal analysis (equal); Investigation (equal); Writing – review & editing (equal). **Stephen Polly:** Investigation (equal); Writing – review & editing (equal). **Erdong Wang:** Investigation (equal); Writing – review & editing (equal). **Seth M. Hubbard:** Investigation (equal); Writing – review & editing (equal). **Marcy L. Stutzman:** Writing – review & editing (supporting). **Joseph Michael Grames:** Investigation (equal); Writing – review & editing (equal).

DATA AVAILABILITY

The data that support the findings of this study are available from the corresponding author upon reasonable request.

REFERENCES

[1]T. Maruyama, E. L. Garwin, R. Prepost, and G. H. Zapalac, Phys. Rev. B **46**(7), 4261 (1992).
[2]K. A. Aniol, D. S. Armstrong, T. Averett *et al.*, Phys. Rev. C **69**, 065501 (2004).
[3]D. S. Armstrong, J. Arvieux, R. Asaturyan *et al.*, Phys. Rev. Lett. **95**, 092001 (2005).
[4]D. Androic, D. S. Armstrong, A. Asaturyan *et al.*, Phys. Rev. Lett. **111**, 141803 (2013).

[5]C. J. Horowitz, S. J. Pollock, P. A. Souder, and R. Michaels, Phys. Rev. C **63**, 025501 (2001).
[6]A. J. R. Puckett, E. J. Brash, M. K. Jones *et al.*, Phys. Rev. C **96**, 055203 (2017).
[7]A. Accardi, J. L. Albacete, M. Anselmino *et al.*, "Electron ion collider: The next QCD frontier—Understanding the glue that binds us all," arXiv:1212.1701 (2014).
[8]W. Liu, Y. Chen, W. Lu, A. Moy, M. Poelker, M. Stutzman, and S. Zhang, Appl. Phys. Lett. **109**, 252104 (2016).
[9]T. Maruyama, E. L. Garwin, R. Prepost, G. H. Zapalac, J. S. Smith, and J. D. Walker, Phys. Rev. Lett. **66**(18), 2376 (1991).
[10]P. J. Orders and B. F. Usher, Appl. Phys. Lett. **50**(15), 980 (1987).
[11]T. Omori, Y. Kurihara, Y. Takeuchi, M. Yoshioka, T. Nakanishi, S. Okumi, M. Tsubata, M. Tawada, K. Togawa, Y. Tanimotol, C. Takahashi, T. Baba, and M. Mizuta, Jpn. J. Appl. Phys., Part 1 **33**(10R), 5676 (1994).
[12]A. Accardi, A. Afanasev, I. Albayrak *et al.*, Eur. Phys. J. A **57**, 261 (2021).
[13]R. E. Welser, S. J. Polly, A. K. Sood, S. M. Hubbard, and K. H. Montgomery, in *IEEE 46th Photovoltaic Specialists Conference (PVSC)* (IEEE, 2019), p. 2642.
[14]A. G. Zhuravlev, V. S. Khoroshilov, and V. L. Alperovich, "Electron emission from Cs/GaAs and GaAs(Cs, O) with positive and negative electron affinity," JEPT Lett. **105**, 686 (2017).
[15]G. Guisbiers, M. Wautelet, and L. Buchaillot, Phys. Rev. B. **79**, 155426 (2009).
[16]A. Addamiano, J. Am. Chem. Soc. **82**(7), 1537 (1960).
[17]S. Polly, B. Bogner, A. Fedorenko, N. Pokharel, P. Ahrenkiel, S. Chowdhury, D. Biswas, and S. Hubbard, Cell Rep. **4**(6), 101432 (2023).
[18]R. S. Goldman, K. L. Kavanagh, H. H. Wieder, S. N. Ehrlich, and R. M. Feenstra, J. Appl. Phys. **83**(10), 5137 (1998).
[19]J. L. McCarter, M. L. Stutzman, K. W. Trantham, T. G. Anderson, A. M. Cook, and T. J. Gay, Nucl. Instrum. Methods Phys. Res. Sec., A **618**, 30 (2010).
[20]R. L. Bell, *Negative Electron Affinity Devices* (Clarendon, Oxford, England, 1973).
[21]O. Watanabe, T. Nishitani, K. Togawa, Y. Takashima, T. Nakanishi, Y. Takeda, and H. Kobayakawa, AIP Conf. Proc. **570**(1), 1024 (2001).
[22]T. Maruyama, D. A. Luh, A. Brachmann, J. E. Clendenin, E. L. Garwin, S. Harvey, J. Jiang, R. E. Kirby, C. Y. Prescott, R. Prepost, and A. M. Moy, Appl. Phys. Lett. **85**, 2640 (2004).
[23]X. G. Jin, B. Ozdol, M. Yamamoto, A. Mano, N. Yamamoto, and Y. Takeda, Appl. Phys. Lett. **105**, 203509 (2014).